



OPEN

Design and synthesis of a novel quinoline thiazolidinedione hybrid as a potential antidiabetic PPAR γ modulator

Ayman M. Ibrahim¹, Mai E. Shoman², Radwa Taher Mohie el-dien³, Entesar Ali Saber⁴, Mahmoud Abdelnaser⁵, Sherif A. Maher⁶, Alaa M. Hayallah^{7,8✉}, Mahmoud Abdul-Aziz El-Rehany⁵ & Gamal El-Din A. Abuo-Rahma^{1,2✉}

Peroxisome proliferator-activated receptor γ (PPAR γ) remains a critical target for antidiabetic drug development due to its role in glucose and lipid metabolism. However, the adverse effects associated with full agonists of the thiazolidinedione (TZD) class, such as weight gain and hepatotoxicity, limit their clinical utility. Herein, we report the design and synthesis of (Z)-5-benzylidene-3-((2-chloroquinolin-3-yl)methyl)thiazolidine-2,4-dione (compound 7), a novel TZD derivative that functions as a potential PPAR γ modulator. Compound 7 reduced blood glucose level (BGL) by 22.33% after 15 days of treatment with a daily single oral dose, demonstrating an antidiabetic effect comparable to TZDs. Additionally, it elevated PPAR γ expression to 75% of the activation level induced by Pioglitazone (PIO). Further characterization of its safety profile reveals that compound 7 is safer on the liver compared to PIO, as alanine transaminase (ALT) and aspartate transaminase (AST) levels remained significantly lower (147.4 ± 4.2 IU/L and 229.9 ± 2.7 IU/L, respectively). Moreover, compound 7 exerts a protective effect on hepatic and pancreatic tissues. Computational metabolic studies predict that compound 7 does not produce toxic metabolites or undergo hydrolysis of the TZD ring, contributing to its improved safety. The docking of Compound 7 into the PPAR γ ligand-binding domain (LBD) demonstrates a unique binding mode, positioning it centrally within the LBD and interacting with key amino acids critical for selective modulation. These findings emphasize the potential of compound 7 as a selective PPAR γ modulator to dissociate insulin-sensitizing effects from adverse side effects, offering a safer alternative to current TZD-based therapies.

Keywords Quinoline, Thiazolidinedione, PPAR γ , Antidiabetic, SPPARMs

Abbreviations

AC	Apical acidophilia
AF2	Activation function 2
ALT	Alanine transaminase
AST	Aspartate transaminase
BBB	Blood brain barrier
BC	Bile canaliculi
BGL	Blood glucose level
CMC	Carboxy methyl cellulose
CNS	Central nervous system

¹Department of Pharmaceutical Chemistry, Faculty of Pharmacy, Deraya University, New Minia 61111, Egypt.

²Department of Medicinal Chemistry, Faculty of Pharmacy, Minia University, Minia 61519, Egypt. ³Department of Pharmacognosy, Faculty of Pharmacy, New Valley University, El-kharga City, Egypt. ⁴Department of Medical science, Histology and Cell Biology, Faculty of Pharmacy, Deraya University, New Minia 61111, Egypt.

⁵Department of Biochemistry, Faculty of Pharmacy, Deraya University, New Minia 61111, Egypt. ⁶Department of Biochemistry, Faculty of pharmacy, New Valley University, El-kharga City, Egypt. ⁷Department of Pharmaceutical Organic Chemistry, Faculty of Pharmacy, Assiut University, Assiut 71526, Egypt. ⁸Pharmaceutical Chemistry Department, Faculty of Pharmacy, Sphinx University, New Assiut, Egypt. ✉email: alaa_hayalah@yahoo.com; gamal.aborahma@mu.edu.eg; gamal.aborahma@deraya.edu.eg

Ct	Threshold cycle
CV	Central veins
CYP	Cytochrome
CYP450	Cytochrome P450
DS	Discovery Studio
ESI	Electrospray ionization
GAPDH	Glyceraldehyde-3-phosphate dehydrogenase
GI	Gastrointestinal
GSH	Glutathione
H	Helix
H&E	Hematoxylin and eosin
IL	Islets of Langerhans
ILD	Interlobular ducts
LBD	Ligand-binding domain
LD	Intralobular ducts
NASH	Nonalcoholic steatohepatitis
NIDDM	Non-insulin-dependent diabetes mellitus
NIH	National Institutes of Health
P	Probability
PA	Portal areas
PAINS	Pan-assay interference compounds
PCOS	Polycystic ovarian syndrome
P-gp	P-glycoprotein
PIO	Pioglitazone
PPAR γ	Peroxisome proliferator-activated receptor γ
PPREs	PPAR response elements
qRT-PCR	Real-time polymerase chain reaction
RMSD	Root mean square deviation
RXR	Retinoid X receptor
SAR	Structure-activity relationship
SPPARMs	Selective PPAR γ modulators
T2DM	Type II diabetes mellitus
TLC	Thin layer chromatography
TMS	Tetramethylsilane
TZD	Thiazolidinedione

Type II diabetes mellitus (T2DM) stands as a chronic metabolic disorder characterized by insulin resistance and impaired glucose homeostasis¹. The therapeutic management of T2DM involves various drug classes, each targeting distinct aspects of glucose regulation. Among them, glitazones (Fig. 1), or thiazolidinediones (TZDs), have emerged as pharmacological agents that modulate insulin sensitivity and improve glycemic control².

TZDs effectively lower hemoglobin A1c by approximately 1% as monotherapy in T2DM without causing hypoglycemia, unlike insulin or insulin secretagogues such as sulfonylureas; this makes them suitable for combination therapy with other antidiabetic agents³. Studies have shown that TZDs improved insulin sensitivity, where the randomized controlled trial has demonstrated that Rosiglitazone is more durable glycemic control compared to metformin or sulfonylurea⁴. Current practice guidelines approved PIO for biopsy-proven nonalcoholic steatohepatitis (NASH), while guidelines recommend TZDs to decrease androgen levels, enhance ovulation, and improve glucose tolerance in women with polycystic ovarian syndrome (PCOS), though not for first-line use in treating hirsutism or infertility⁵.

The primary molecular target of glitazones in antidiabetic action is the PPAR γ ⁶. PPAR γ is a nuclear receptor that plays a crucial role in regulating glucose and lipid metabolism in various tissues, including adipose tissue,

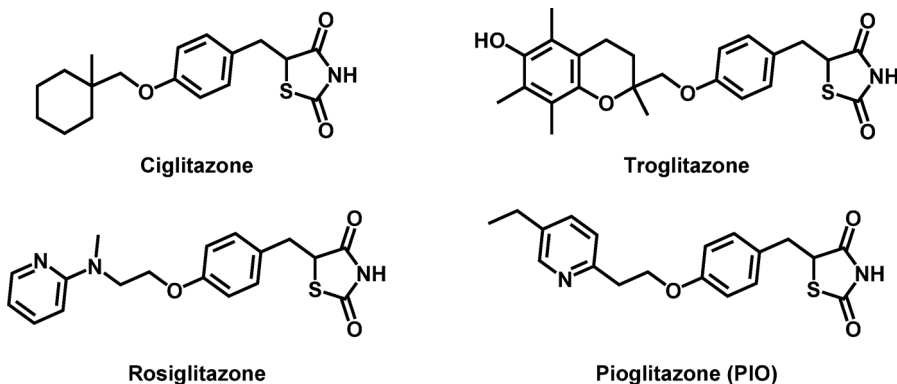


Fig. 1. Chemical structures of glitazones.

skeletal muscles, and liver^{7,8}. Upon activation by TZDs, PPAR γ forms a heterodimer with Retinoid X Receptor (RXR) and binds to specific PPAR response elements (PPREs) in the promoter region of target genes⁹. This activation results in the transcriptional regulation of pathways involved in insulin sensitivity, adipogenesis, and lipid metabolism, leading to improved glucose homeostasis^{10,11}. TZDs are full agonists of PPAR γ that form hydrogen bonds between their TZD head group and the ligand-binding domain (LBD) of PPAR γ , specifically with the side chains of key residues His323, His449, and Tyr473 (Fig. 2). These interactions play a crucial role in stabilizing helix 12 (H12) in the active conformation leading to the formation of the activation function 2 (AF2) surface, which is necessary for full receptor activation¹².

Despite their efficacy, glitazones are associated with a range of adverse effects, including weight gain and fluid retention. Long-term use of PIO raises concerns about cardiovascular safety, particularly an increased risk of heart failure and myocardial infarction¹³. PIO may elevate the risk of bone fractures and has been linked to cases of liver toxicity. Moreover, long-term use of PIO has also been linked to an increased risk of bladder cancer, raising concerns about safety profile^{14,15}. Three TZDs received FDA approval: Troglitazone, Rosiglitazone, and PIO. Troglitazone was introduced in 1997 but withdrawn in 2000 due to liver toxicity concerns. Rosiglitazone and Pioglitazone were both approved in 1999, but Rosiglitazone faced restrictions due to cardiovascular concerns that were later lifted⁵.

Thus, a new prospective class of compounds appeared for the treatment of diabetes as selective PPAR γ modulators (SPPARMs) (Fig. 3). These compounds have been demonstrated to retain favorable insulin-sensitizing effects while exhibiting little to no adverse effects. SPPARMs induce selective receptor conformations, engaging distinct signaling pathways, which leads to a more targeted and balanced activation of PPAR γ ¹⁶. This selective modulation enhances insulin sensitivity while minimizing common side effects such as weight gain, fluid retention, and cardiovascular risks, making them a safer alternative to traditional TZDs¹⁷.

SPPARMs, as shown in Fig. 3, do not share a general structure. However, they exhibit common binding features within the PPAR γ LBD (Fig. 4). For example, INT131, a well-characterized SPPARM, binds to the LBD in a manner representative of this class¹⁸. Like other SPPARMs, INT131 interacts hydrophobically with Cys285 of H3, a critical residue for partial activation, and engages Arg288 via hydrophobic/van der Waals forces (Fig. 4A). These interactions are often mediated by aromatic groups present within the SPPARM structure, as shown in Fig. 4B. This contrasts with full agonists like PIO, which stabilize the AF2 domain through strong electrostatic interactions with His323, Tyr473, and His449. The distinct binding mode of INT131 (Fig. 4A) exemplifies the SPPARM signature: retention of key interactions with Cys285 and Arg288, coupled with the absence of direct stabilization of the AF2 domain. These features collectively contribute to the unique partial activation profile and reduced adverse effects associated with SPPARMs.

Therefore, motivated by the advantages of the SPPARMs, a novel derivative of the TZD scaffold has been designed with improved pharmacological properties. The design of this compound was based on several considerations. The investigations showed that toxicity of TZDs is most likely due to the hydrolysis of the TZD ring leading to formation of reactive intermediates, and hence TZD toxicity¹⁹. Additionally, it was observed that substitution at the nitrogen atom of the TZD ring in GQ-11 prevents the cleavage of the TZD moiety, rendering it non-toxic to the liver²⁰. Based on these observations, the first consideration was to modify the TZD ring in the desired compound by introducing a substitution at the nitrogen atom.

The other consideration is to enhance the designed compound's binding with its target. A quinoline ring was selected as the nitrogen substituent. The aromatic nature of quinoline, characterized by its π -electron system, enables π - π stacking interactions with aromatic residues in the binding sites of biomolecules. Within the LBD of PPAR γ , these interactions possible to occur with aromatic residues, including Phe282, Phe363, and His449. Additionally, the nitrogen atom within the quinoline ring contributes to hydrogen bonding, enhancing specificity and affinity for target binding sites²¹.

The final point depends on the selection of 5-benzylidene-2,4-thiazolidinedione moiety over 5-benzyl counterpart. The presence of the exocyclic double bond eliminates concerns regarding stereochemical instability and potential racemization. This structural preference facilitates access to the target compound without complexities associated with reduction methods of double bond as non-selectivity over other functional groups,

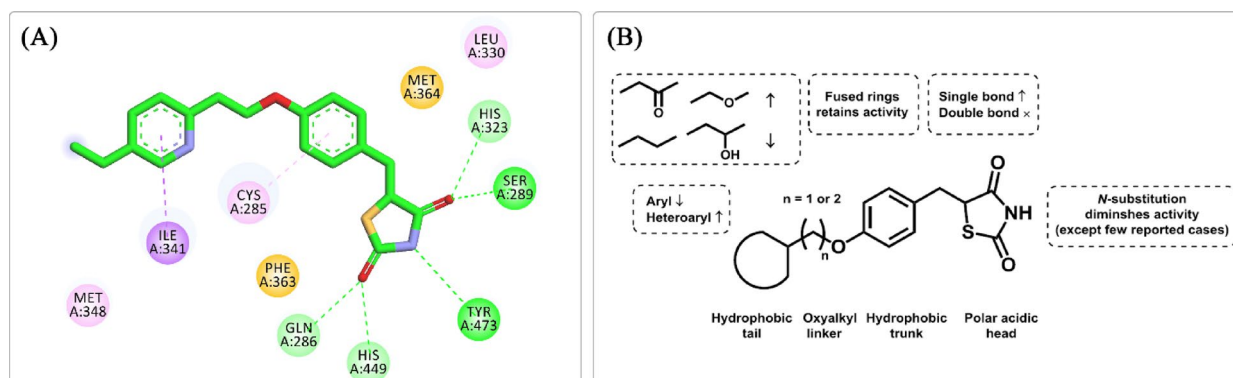
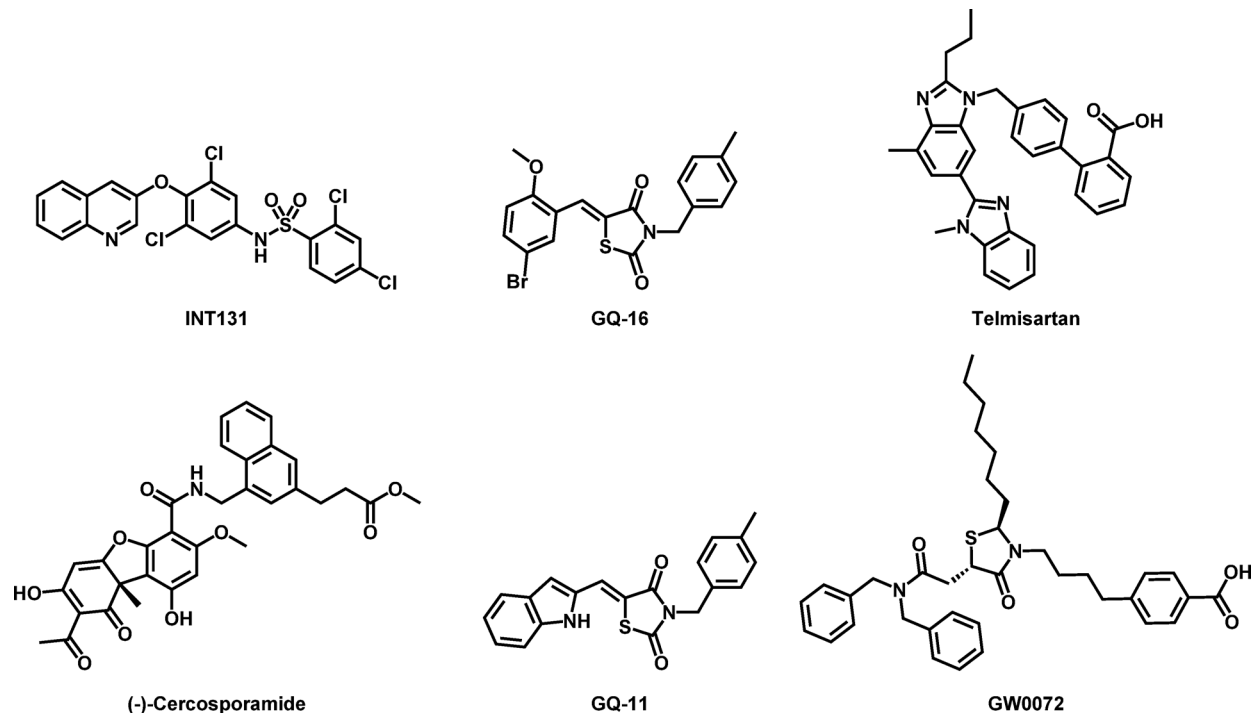
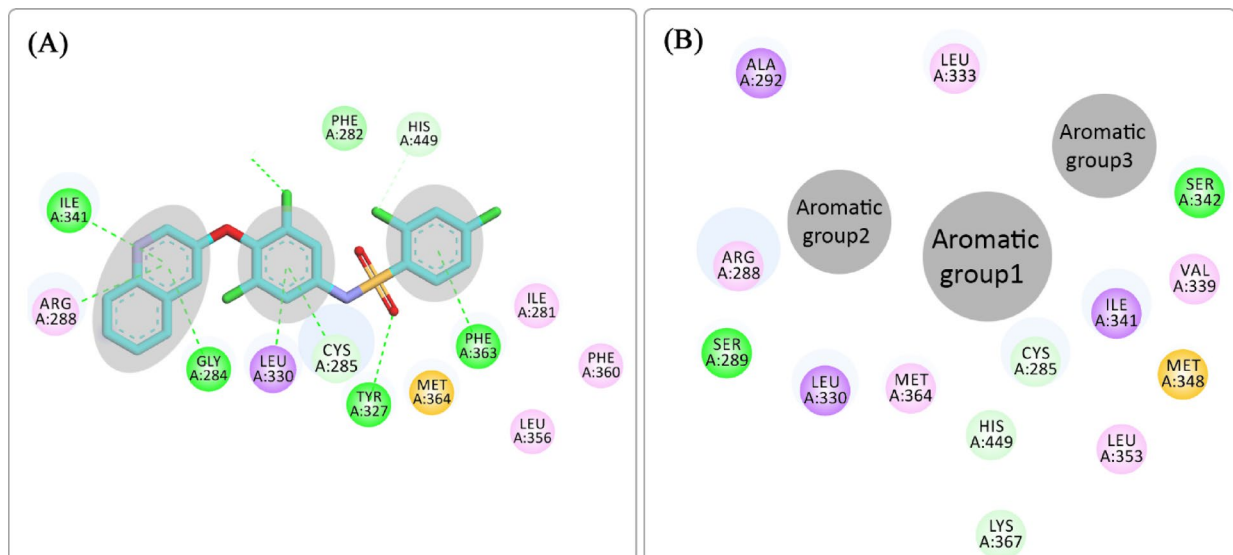


Fig. 2. (A) Binding mode of PIO with key residues of PPAR γ LBD. (B) Structure-activity relationship (SAR) of TZDs as PPAR γ full agonists.

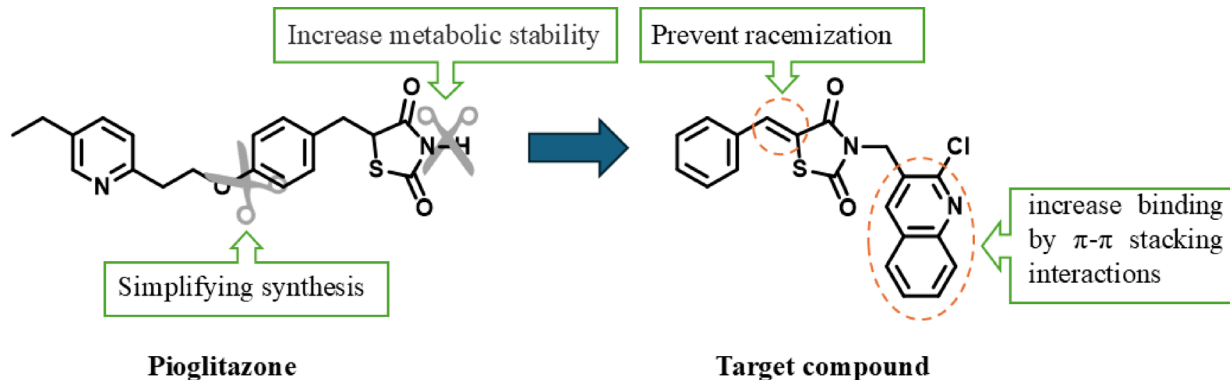
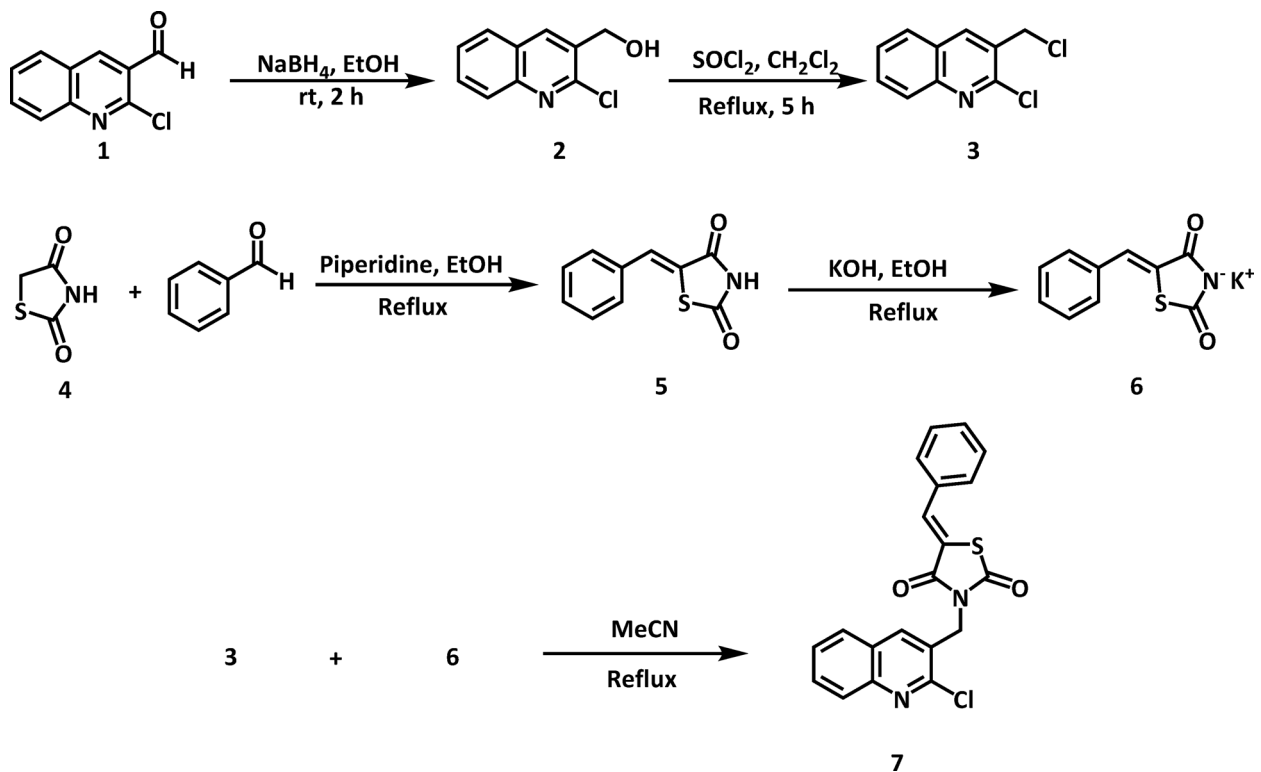
**Fig. 3.** Chemical structures of SPPARMs.**Fig. 4.** (A) Binding mode of INT131 with key residues of PPAR LBD γ . (B) General structure features of SPPARMs.

toxicity, catalyst poisoning, and low to moderate yield. Combining these structural features, compound 7 was developed to achieve an optimized balance of safety, efficacy, and drug-like properties (Fig. 5)²².

Results and discussion

Chemistry

The titled compound 7 was synthesized as per the route outlined in Fig. 6. Acetanilide was treated with Vilsmeier–Haack reagent (POCl_3 and N,N -dimethyl formamide (DMF)) to form intermediate 1. Intermediate 1 was then treated with solid NaBH_4 in ethanol to afford 2-chloro-3-hydroxymethylquinoline 2, followed by chlorination with SOCl_2 in dichloromethane to obtain intermediate 3. Heating intermediate 3 in acetonitrile under reflux with the potassium salt of (*Z*)-5-benzylidenethiazolidine-2,4-dione 6 formed the target compound 7. The structure of

**Fig. 5.** The design of the target molecule.**Fig. 6.** Synthetic pathway of target compound 7.

TZD derivatives 7 was confirmed by ¹H and ¹³C NMR. For instance, the ¹H NMR spectrum of compound 7 was characterized by a singlet signal assigned to the methylene protons (CH_2) which experienced a downfield shift from δ 4.82 to 5.00 ppm (Figure S1). Notably, a characteristic signal for the methylene group appeared at δ 42.60 ppm. Moreover, the chemical shift of the methine proton shifted from δ 7.79 to 7.97 ppm. Also, the spectrum included a singlet at δ 8.40 ppm, corresponding to the H4 of the quinoline moiety. Another signal at δ 8.03 ppm represents the proton H5 of the quinoline nucleus. Additionally, a signal at δ 7.94 ppm corresponds to H8 of the quinoline moiety. The spectrum also exhibited a triplet at δ 7.79 ppm, representing H7 of the quinoline group. Furthermore, multiple resonances were observed for the phenyl group, including a multiplet at the range δ 7.54–7.64 ppm. DEPTQ-135 ¹³C NMR spectrum of compound 8a displayed 18 distinct signals (Figure S2). Among these signals, 9 signals were observed exhibiting a phase shift of 180° compared to the other 9 signals arising from CH and CH_3 carbons. Notably, a characteristic signal originating from the methylene group appeared at δ 42.60 ppm. The peaks observed at 167.41 and 165.50 ppm were attributed to the two carbonyl groups present in the TZD ring. The molecular structure was further confirmed by mass spectrometry (ESI-MS, water), showing the molecular ion peak $[\text{M} + \text{H}]^+$ at m/z 380.5, consistent with the calculated molecular mass (Figure S3). The peak at m/z 434 could potentially be attributed to an adduct with the solvent, specifically $[\text{M} + \text{Na} + \text{MeOH}]^+$. Crucially, the expected chlorine isotope peak at m/z 382.5 was also observed, with an intensity of approximately

32% relative to the $[M + H] + 380.5$ peak, confirming the presence of the chlorine atom in the molecule. HPLC analysis of compound 7 revealed a purity level of 95% (Figure S4). The synthesis of compound 7 is notably simpler and more straightforward, with a higher yield compared to the synthesis of PIO^{23,24}. It involves fewer steps and relies on inexpensive and commercially available starting materials, making it a cost-effective and practical approach for large-scale production.

Biological investigation

In vivo antidiabetic activity

Compound 7 was evaluated on alloxan-induced diabetic rats for its blood glucose lowering effect. Besides control and diabetic groups, PIO was used as a reference drug with a single oral dose (36 mg/kg) to group III²⁵. Compound 7 was also orally administered as an equimolar (1 mmole) single dose (38 mg/kg) to group IV. PIO and 7 were given in the form of a 0.25% carboxymethylcellulose (CMC) suspension and the fasting BGLs were monitored as per standard protocols on the 0-day, 1st, 7th, and 15th day of the commencement of the experiment^{25,26}. The results are outlined in Fig. 7.

The data analysis showed that compound 7 and PIO effectively reduced blood glucose levels. On the 15th day, compound 7 demonstrated a decrease in BGL from 300 ± 2.23 mg/dL to 233 ± 5.05 mg/dL, while PIO exhibited a BGL reduction from 260 ± 3.5 mg/dL to 134 ± 7.74 mg/dL, in comparison to the diabetic group. Thus, compound 7 showed a promising blood glucose lowering effect with 22.33% along with the reference drug, PIO (48.46%).

PPAR γ gene expression study

PPAR γ gene expression analysis was done to evaluate the impact of compound 7 on modulating PPAR γ gene. As shown in Fig. 8, diabetes significantly downregulated the expression of PPAR γ gene, compared to the normal control group. However, in both 7-treated group and PIO-treated group, the expression of PPAR γ gene was markedly elevated, in contrast to the diabetic group. Thus, the increase in gene expression exerted by compound 7 supports its blood glucose lowering effect and its potential PPAR γ activation. The transcriptional activity induced by SPPARMs is lower than that of full agonists. For instance, some partial agonists show transcriptional outputs ranging from 20 to 80% of full agonists like Rosiglitazone in reporter assays²⁷. This partial activation modulates a subset of PPAR γ -regulated genes, focusing on those involved in insulin sensitization while minimizing the activation of genes linked to adverse effects.

Body weight gain study

Due to the earlier association of PPAR γ full agonists with weight gain among treated animals, compound 7 was further analyzed for body weight gain (Fig. 9). In the diabetic control group, the body weight was decreased which may be attributed to the underlying diabetic condition. Administration of compound 7 resulted in a slight increase in body weight indicating that compound 7 has no significant effect on body weight compared to both the normal and diabetic control groups. In comparison, treatment with PIO induced a significant weight gain, which was notably higher than the changes observed with compound 7 and the normal control group.

Hepatotoxicity studies

Compound 7 was further analyzed for an increase or decrease in the levels of ALT and AST (Fig. 10). Normal control group showed ALT and AST levels of 113.2 ± 3.2 and 124.8 ± 4.4 IU/L, respectively. The diabetic control

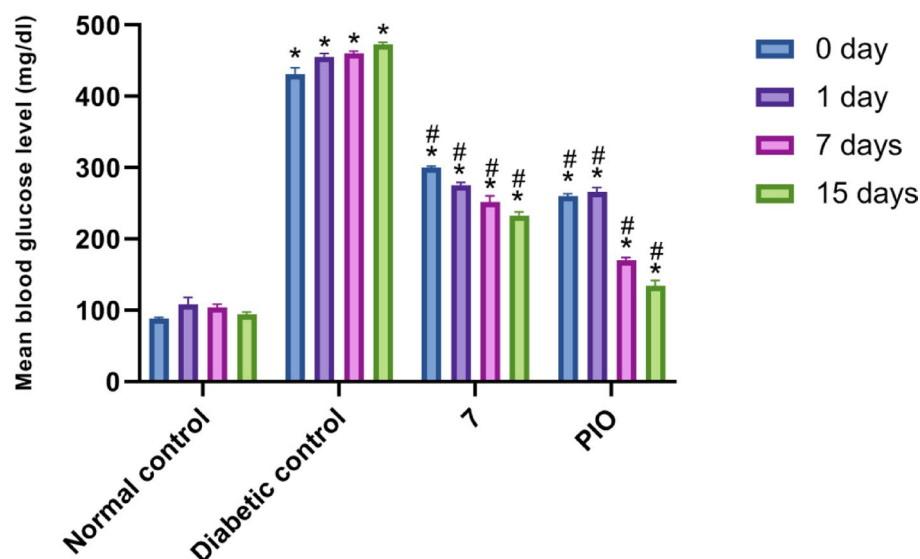


Fig. 7. Antidiabetic activity of compound 7 in alloxan-induced diabetic rats. Data are analyzed by one-way ANOVA followed by Bonferroni *t*-test and expressed as mean \pm SD from five observations; * $p < 0.05$ versus normal control; # $p < 0.05$ versus diabetic control.

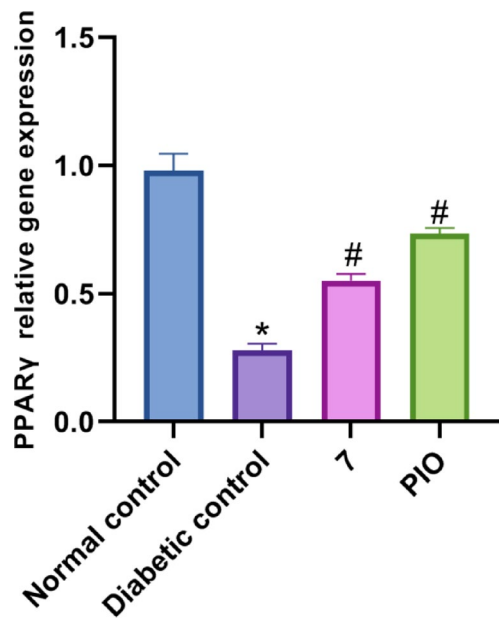


Fig. 8. Effect of compound 7 on pancreatic PPAR γ mRNA levels. Data are analyzed by one-way ANOVA followed by Bonferroni *t*-test and expressed as mean \pm SD from five observations; * $p < 0.05$ versus normal control; and # $p < 0.05$ versus diabetic control.

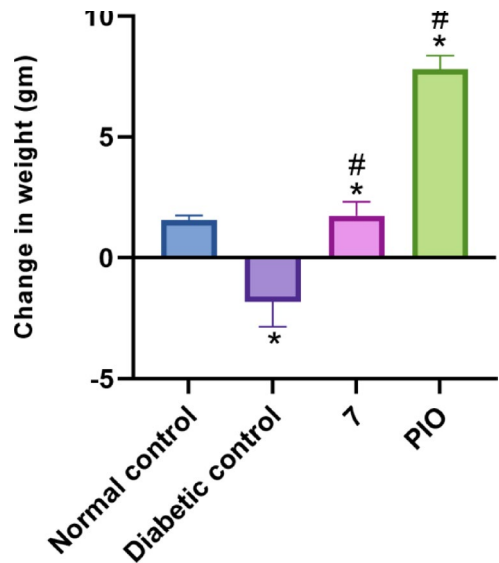


Fig. 9. Effect of compound 7 on body weight gain in rats. Data are analyzed by one-way ANOVA followed by Bonferroni *t*-test and expressed as mean \pm SD from five observations; * $p < 0.05$ versus normal control; and # $p < 0.05$ versus diabetic control.

group served as a model for evaluating the impact of diabetes on liver function. The levels of ALT and AST were significantly elevated to 147.4 ± 4.2 IU/L and 229.9 ± 2.7 IU/L, respectively. This increase indicates impaired liver function associated with diabetes. Compound 7 was effective in bringing down the levels of ALT and AST to the normal range, with 124.3 ± 5.3 IU/L and 123.3 ± 7.6 IU/L, respectively. Treatment with PIO resulted in an elevated level of AST (154.7 ± 4.8 IU/L) when compared to the normal control group.

Histopathological examination of liver sections from the normal control group demonstrated normal hepatic architecture with characteristic hexagonal lobules. The tissue showed well-organized hepatic cords radiating from central veins, with intact portal triads at the periphery. Hepatocytes exhibited normal polyhedral morphology with vesicular nuclei and acidophilic cytoplasm, separated by clear sinusoidal spaces (Fig. 11A1, A2).

Liver sections from the diabetic control group exhibited severe disruption of hepatic architecture with disorganized hepatic cords and prominent sinusoidal dilation. Hepatocytes displayed extensive degenerative

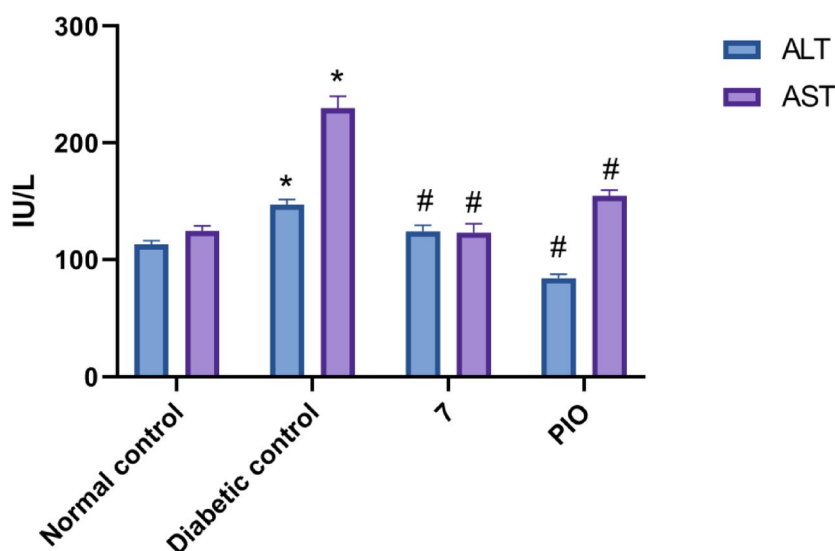


Fig. 10. Effect of compound 7 on serum AST and ALT levels. Data are analyzed by one-way ANOVA followed by Bonferroni *t*-test and expressed as mean \pm SD from five observations; * $p < 0.05$ versus normal control; and # $p < 0.05$ versus diabetic control.

changes, including cytoplasmic vacuolation and nuclear abnormalities (pyknosis, fragmentation, and karyolysis). Dilated sinusoids, steatosis, glycogen depletion, and enlarged Kupffer cells were present. Notable features included marked central vein congestion, patchy necrosis, and perivenular inflammatory cell infiltration extending toward portal areas. These pathological changes indicate the severity of diabetes-induced hepatic injury (Fig. 11B1, B2).

Treatment with compound 7 demonstrated notable amelioration of diabetes-induced hepatic changes. The liver sections showed improvement in hepatic architecture, with partially restored hexagonal lobular structure and organized central veins. Hepatocytes exhibited improved cellular integrity, radiating in well-defined cords from the central axis. The hepatic tissue displayed reduced inflammatory infiltration compared to the diabetic control group, with only mild collagen deposition in the interlobular septa and around sinusoids, indicating attenuation of diabetes-induced liver damage (Fig. 12A1-A3).

PIO treatment demonstrated moderate amelioration of alloxan-induced hepatic changes. The liver sections showed partial restoration of hepatic architecture, with hepatocytes arranged in radiating cords and relatively normal portal areas. While most hepatocytes displayed normal acidophilic cytoplasm and vesicular nuclei, scattered cells exhibited mild vacuolation. The tissue showed reduced inflammatory infiltration compared to diabetic controls, with minimal fibrous tissue surrounding hepatic lobules, central veins, and portal areas. Notable features included prominent Kupffer cells along sinusoidal linings and visible bile canaliculi in portal tracts (Fig. 12B1, B2).

It has been proposed that the oxidative cleavage of the TZD ring is a convinced metabolic pathway leading to the formation of reactive intermediates, and hence TZD toxicity. Metabolic studies confirmed this perception by the presence of S-oxidized metabolites of Troglitazone, PIO, and Rosiglitazone^{28–30}. The proposed mechanism from these studies depicted by initial CYP450-mediated S-oxidation of TZD leading to formation of an unstable TZD sulfoxide. Then, the formed intermediate undergoes spontaneous cleavage to a reactive α -keto isocyanate intermediate. This isocyanate intermediate is more likely to covalently bind to hepatic proteins such as glutathione (GSH) and consequently cause hepatic failure.²² In order to predict the metabolic positions on the TZD ring in 7, it was submitted to GLORYx server, a reliable tool for forecasting the metabolites resulting from both phase I and phase II biotransformations³¹. The results provided the atom positions of 7 where metabolic reactions are most likely to initiate by CYP450, ranked by probability of occurrence from highest to lowest (Fig. 13; Table 1).

These results indicated that the sulfur atom would be the primary site of metabolism, with a P of 0.584, while all other atom positions within the TZD exhibited significantly lower probabilities, each falling below 0.1. Other carbons within the quinoline and phenyl rings exhibited a substantially higher probability for metabolic reactions than the TZD moiety. This suggests that the TZD of compound 7 may be less susceptible to metabolic transformations, except sulfur atom.

Furthermore, the investigation extended to the structural elucidation of the predicted metabolites using GLORYx server, depicted in Fig. 14. These predictions revealed that the foremost metabolic transformation involved the oxidation of the sulfur atom M-I, while there were no observed metabolites with a cleaved TZD ring. Subsequently, the second-highest probabilities were associated with hydroxylation reactions at C5, C7, and C8 of the quinoline M-II: M-IV, each possessing an equal likelihood of 0.26, followed by hydroxylation of phenyl group M-V: M-VII (P: 0.25). Interestingly, the analysis also observed the glutathionation process in phase II metabolism via conjugation at the methine group M-VIII, which served as a Michael acceptor, along with C2 of the quinoline moiety M-IX. These results indicated the high possibility of metabolic reactions to locate at sulfur atom through S-oxidation without ring cleavage. This observation may be attributed to the

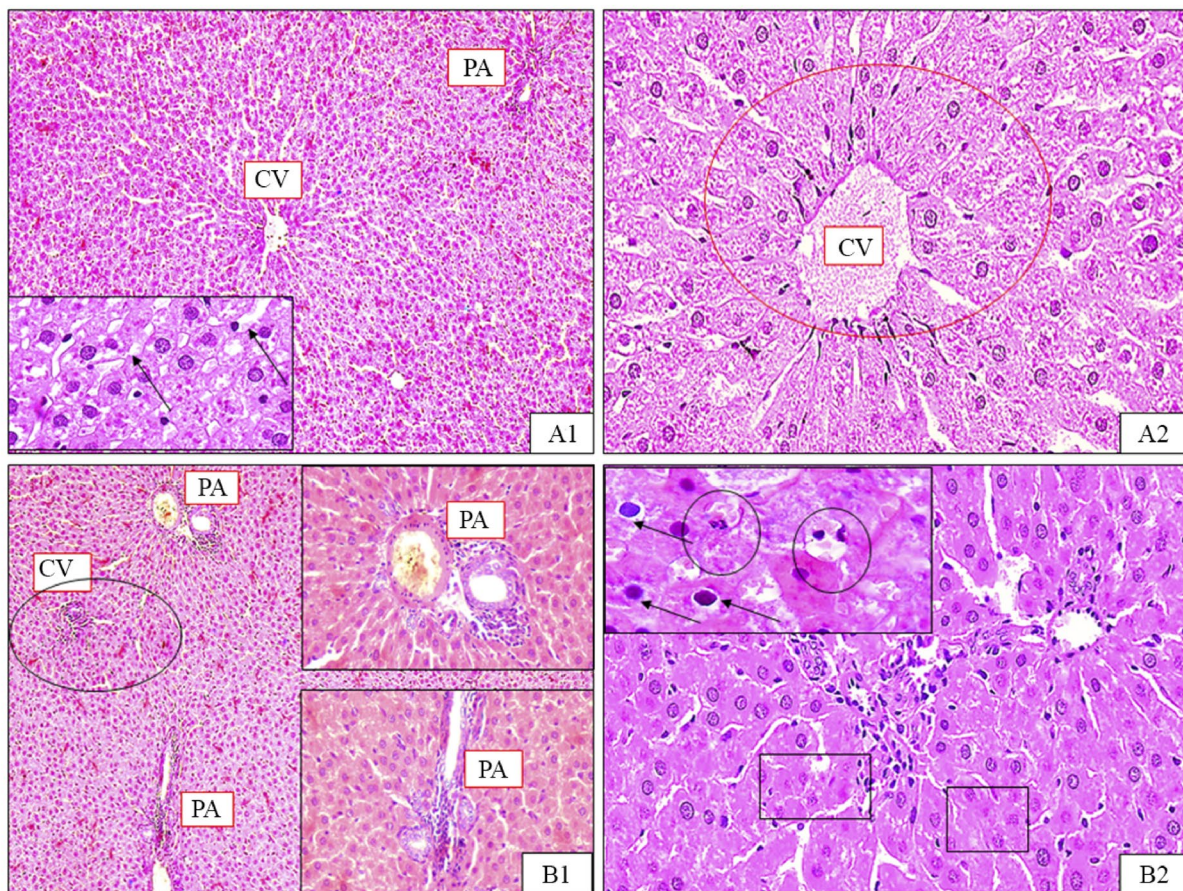


Fig. 11. Photomicrographs of rat liver tissue for normal group (A1 & A2), and diabetic group (B1 & B2). (A1) Normal liver architecture with central veins (CV) and blood sinusoids in-between rows of hepatocytes (arrows). (A2) Hepatocytes are large polyhedral cells with vesicular nuclei and vacuolated and acidophilic cytoplasm. (B1) marked congestion of CV, vessels of the portal areas (PA) and blood sinusoids. Widely distributed patchy inflammation and necrosis mainly concentrated around the central veins (empty circle); (B2) Hepatic cord disorganization and dissolution. Varying degrees of cytoplasmic vacuolation (empty rectangles) and some nuclei showing pyknosis (arrows).

substitution at the nitrogen atom of the TZD moiety, which likely prevents hydrolysis of TZD and consequently the formation of reactive metabolites that could potentially induce toxicity²⁰. These findings reveal that 7 could be less toxic than the current glitazones.

Morphological changes in pancreatic tissue

Histopathological studies were performed to evaluate the effect of 7 and PIO on pancreatic islets. The normal histological structure of the pancreatic tissue appeared in the form of lobules packed with acini that were separated from each other by very little connective tissue septa (Fig. 15A1-A4). It was reported that alloxan causes degeneration and necrosis of pancreatic β -cells^{32,33}. The results showed that diabetic pancreatic tissue was characterized by marked morphological changes in the form of widening of the interlobular connective tissue containing numerous congested blood vessels loaded with RBCs (Fig. 15B1-B5). The inflammatory cells, mainly neutrophils, and eosinophils, were also seen surrounding ducts.

However, the pancreatic tissue of diabetic group treated with PIO showed signs of improvement in tissue organization (Fig. 16A1-A2). The pancreatic lobules appeared more organized with intervening connective tissue. The remaining islets demonstrated better preservation with reduced inflammatory cellular infiltration compared to the diabetic control group. These results agree with studies that demonstrated the protective effects on pancreatic β -cells exerted by PIO³⁴. The pancreatic tissue of 7-treated group showed marked improvement which was observed in the morphological features (Fig. 16B1-B2). The overall tissue architecture appeared more preserved compared to the diabetic control group, except some blood vessels remained congested, and certain ducts showed dilation with retained secretions. The reduction in inflammatory infiltration and better preservation of tissue architecture suggest that compound 7 may exert protective effects on pancreatic tissue similar to PIO, possibly through anti-inflammatory and antioxidant mechanisms. These protective effects could help maintain pancreatic function during the diabetic state, though longer-term studies would be needed to evaluate any potential effects on tissue regeneration.

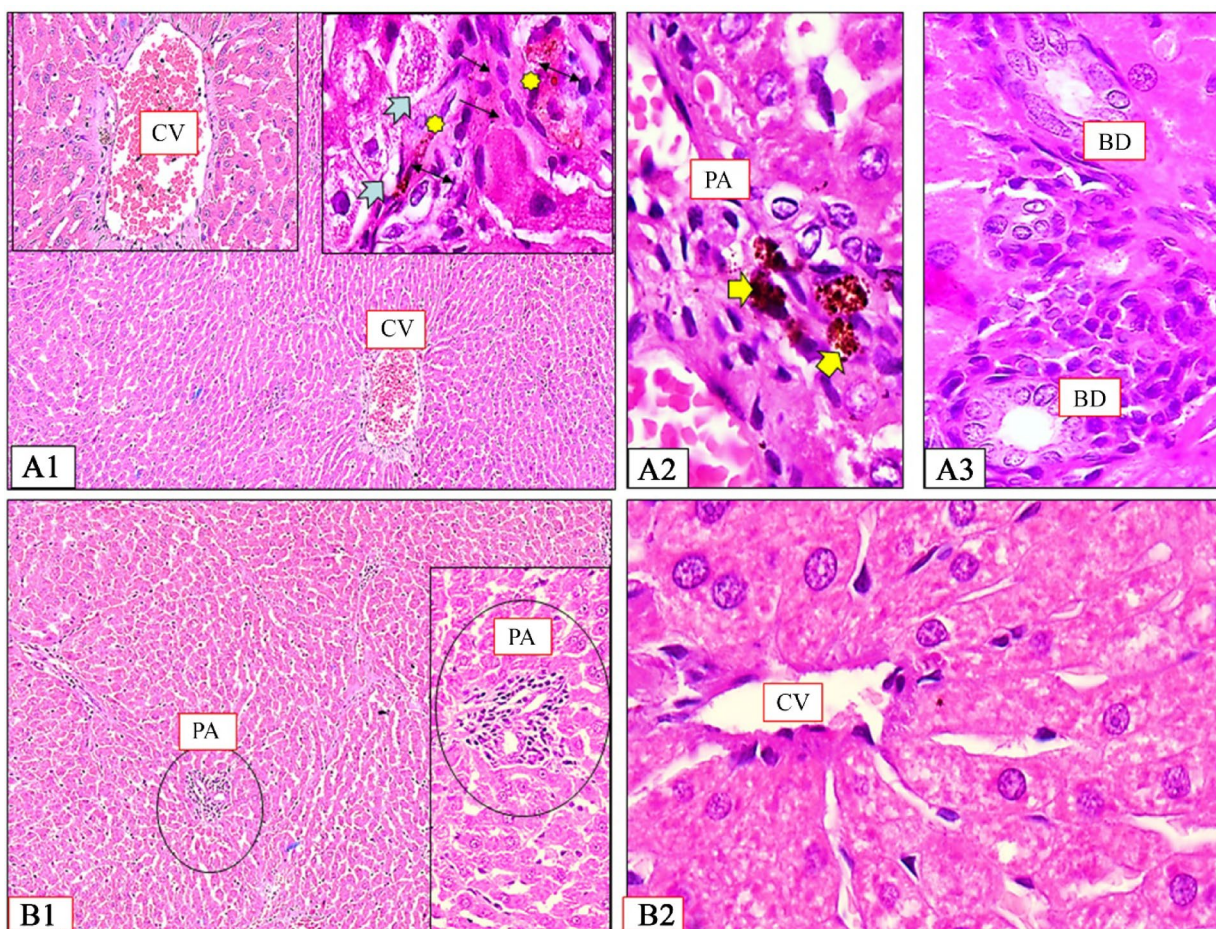


Fig. 12. Photomicrographs of rat liver tissue of 7-treated group (A1-A3) and PIO-treated group (B1 & B2). (A1) Hepatocytes have normal appearance but few hepatocytes appeared slightly vacuolated (tailed arrows). (A2) Kupffer cells appear inserted in the endothelial lining of hepatic sinusoids detected by particles of brown containing pigments (double arrows). (A3) Branching bile canaliculi (BC) seen in portal tracts. (B1) Classic hepatic lobules were roughly hexagonal in shape with CV forming their central axis from which cords of hepatocytes radiating like sun rays and surrounded at each corner by PA. (B2) Delicate collagen fibers in the interlobular septa and surrounding the liver cells and the blood sinusoids.

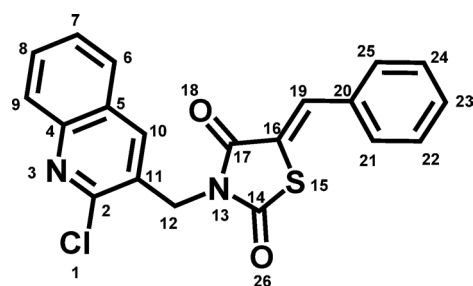


Fig. 13. Chemical structure of compound 7 with its numbering by GLORYx.

Molecular docking study

Molecular docking studies were performed to investigate the binding mode of compound 7 within the PPAR γ LBD, and to compare it with the reference drug PIO. The PPAR γ LBD has a large Y-shaped ligand binding pocket. PIO adopts a U-shaped conformation within the binding site with the hydrophobic chains wrapping around H3. TZD of PIO is reported to exist adjacent to H12 where the nitrogen atom makes a hydrogen bond with the hydroxyl group of Tyr473 in H12, stabilizing the active conformation of H12. Additionally, two carbonyl

Atom	P	Atom	P	Atom	P	Atom	P	Atom	P
S15	0.584	C10	0.092	Cl	0.056	O26	0.016	C22	0.0
C23	0.165	C6	0.092	C14	0.052	C17	0.016	C20	0.0
C9	0.132	C19	0.088	C11	0.036	O18	0.004		
C12	0.12	N3	0.088	C2	0.036	C5	0.004		
C7	0.116	C16	0.056	C25	0.032	C4	0.004		
C8	0.104	N13	0.056	C21	0.032	C24	0.0		

Table 1. The probability of metabolic biotransformation at each position of compound 7 proposed by GLORYx. “P” means probability.

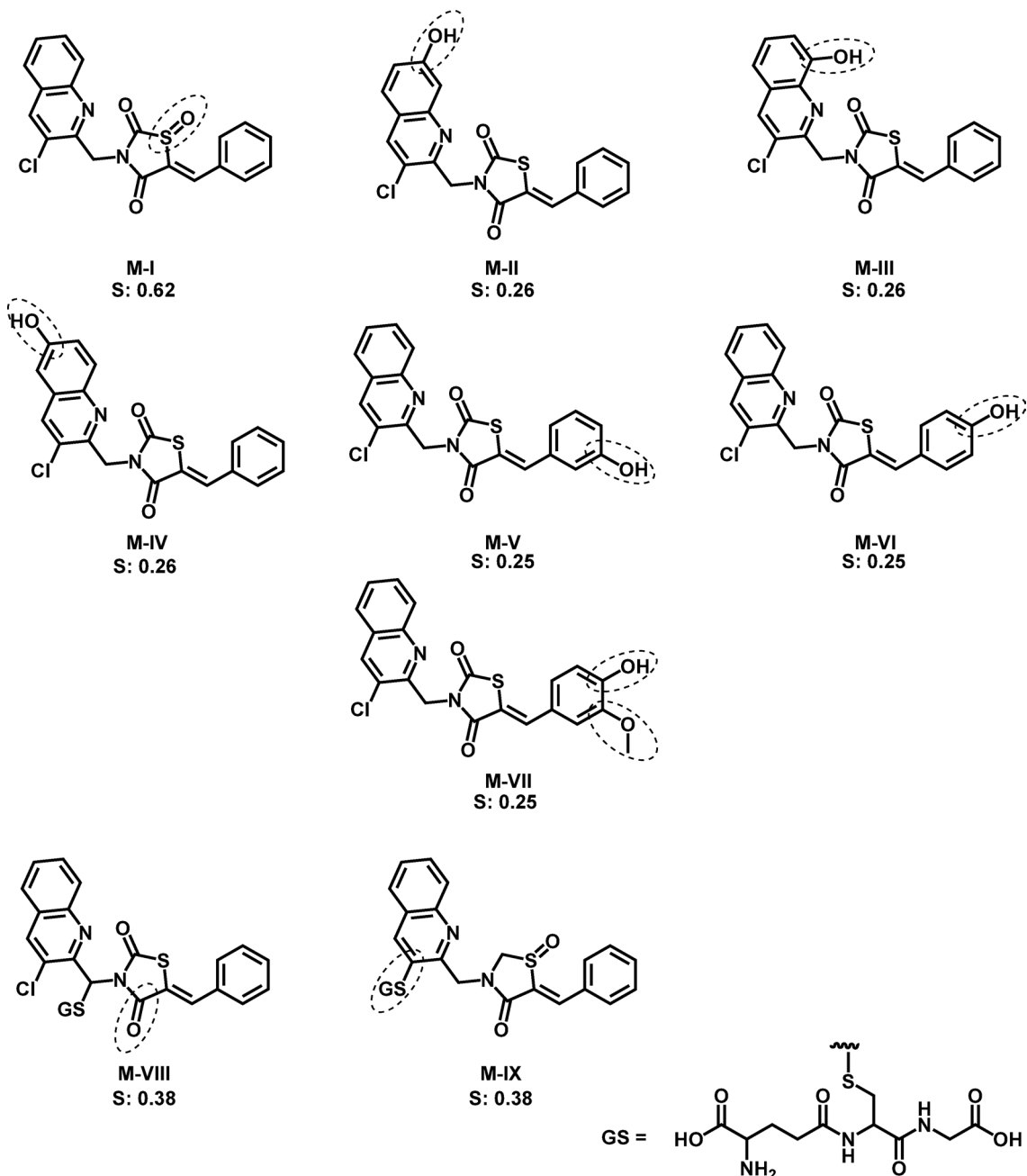


Fig. 14. Predicted metabolic structures of compound 7 through phase I and II using GLORYx.

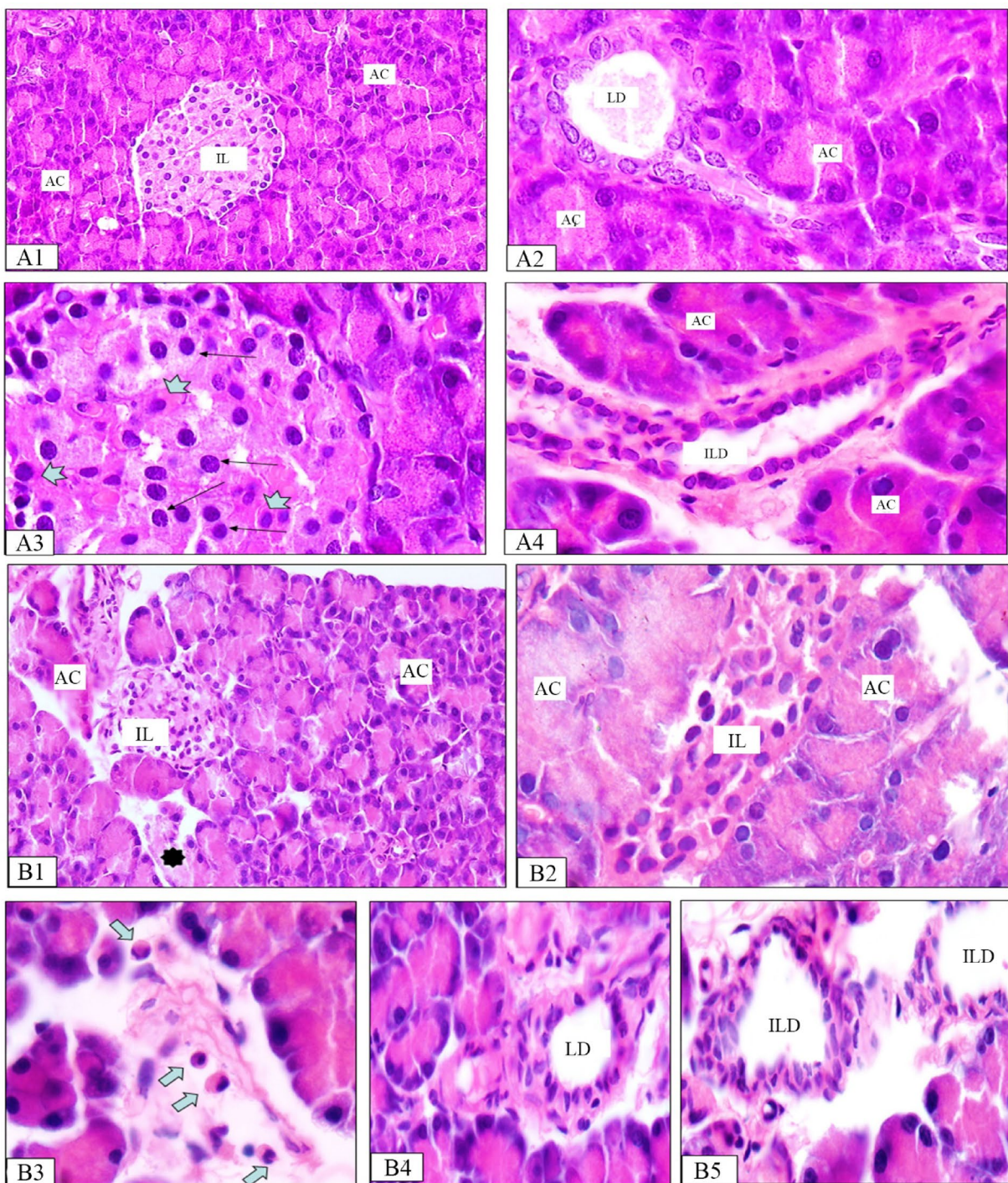


Fig. 15. Photomicrograph of rat pancreatic tissue obtained from normal and diabetic groups and stained with hematoxylin and eosin (H & E). (A1-A4) Control group showing pancreatic acini with its basal basophilia and apical acidophilia (AC), Islets of Langerhans (IL) containing cells that form cords separated by a network of blood capillaries. α -Cells at the periphery (thick arrows) and β -cells at the center (thin arrows). (B1-B3) Diabetic group showing some islet's cells with pyknotic and/or fragmented nuclei. The degenerated cells surrounded by empty spaces were filled with amyloid-like material. Some islets appear completely devoid of cells (black star). (B4-B5) Intralobular and interlobular ducts showed stratification of their epithelial lining (LD & ILD).

groups of the TZD head group make hydrogen bonds with the side chains of His323, Ser289, and His449. The phenyl group of the PIO engaged in hydrophobic interaction with amino acid Cys285³⁵.

Docking studies of compound 7 on PPAR γ , complexed with PIO as a co-crystallized ligand (PDB code: 5Y2O), were performed using AutoDock software. To validate the docking protocol, PIO was re-docked onto

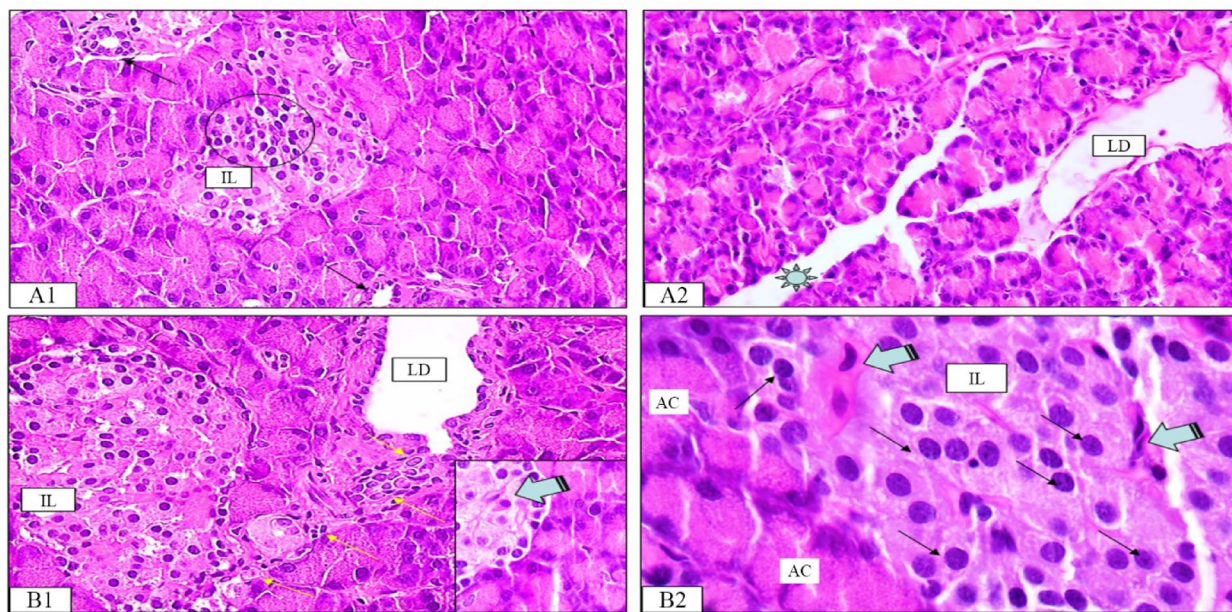


Fig. 16. Photomicrograph of rat pancreatic tissue obtained from PIO- and 7-treated groups and stained with H&E. (A1-A2) PIO-treated group showing scattered areas of small lobules separated by abundant connective tissue. Many islets showed an increase in cellular density, reduction of the inflammatory cellular infiltration, and more numerous β -cells occupying the center of the islets (empty circle). LDs were dilated and lined with flat cells and filled with accumulated secretion. (B1-B2) 7-treated group showing normal pancreatic tissue. The islet cells appeared normal with fibroblast-like cells infiltrating the islets (stripped arrows). An islet showing connection by a stream of cells to the nearby duct that showed nearly normal lining epithelium (yellow arrows).

the binding domain of PPAR γ . PIO docked at almost the same position with a binding score of -9.62 kcal/mol with RMSD equals 1.73 Å.

The docking results also revealed a high binding score for 7 (-9.66 Kcal/mol). The analysis revealed that the binding pose of compound 7 typically lies between arm I and arm II of the PPAR γ binding pocket (Fig. 17). The phenyl ring of compound 7 showed the same interactions with key amino acid Cys285 (arm I), similar to the co-crystallized ligand. The quinoline ring of compound 7 played a critical role in stabilizing the molecule through multiple interactions (arm II). The quinoline ring itself established a π - π stacking interaction with Arg288, while the nitrogen atom of the quinoline moiety formed a hydrogen bond with Glu343. Furthermore, the chloro substituent of the quinoline ring participated in hydrophobic interactions with Leu333, enhancing the compound's affinity in this region of the binding pocket (Fig. 17). Finally, TZD ring formed a network of π -sigma interactions with Leu330 and Arg288, further reinforcing the compound's positioning within the binding pocket.

In silico ADME prediction

The ADME properties of compound 7 were evaluated using the SwissADME server and compared with PIO as a reference drug³⁶. The results (Table S1) confirmed that compound 7 complies with Lipinski's rule of five, with no violations, suggesting favorable oral bioavailability. The pharmacokinetic predictions indicate high gastrointestinal (GI) absorption, further supporting the compound's suitability for oral administration. The blood-brain barrier (BBB) permeability is predicted to be low, suggesting that compound 7 is unlikely to cause central nervous system (CNS)-related side effects. Moreover, compound 7 is not a P-glycoprotein (P-gp) substrate, indicating it is not actively effluxed, which may contribute to improved bioavailability. Furthermore, compound 7 does not trigger any PAINS (Pan-Assay Interference Compounds) alerts. Additionally, the synthetic accessibility score of 3.29 suggests that compound 7 is relatively straightforward to synthesize, supporting its feasibility for synthesis.

Overall, compound 7 shares the same biological profile and binding mode as SPPARMs, offering the benefits of partial receptor activation with reduced adverse effects (Fig. 18). Compound 7 represents a novel and safer alternative to PIO, providing a strong foundation for the future development of improved PPAR γ modulators for diabetes treatment.

Experimental Chemistry

Materials and methods

All required chemicals, solvents, and reagents were purchased from Sigma-Aldrich and Merck. Reaction progress was monitored using thin layer chromatography (TLC) on pre-coated Silica Gel Merck 60 F254

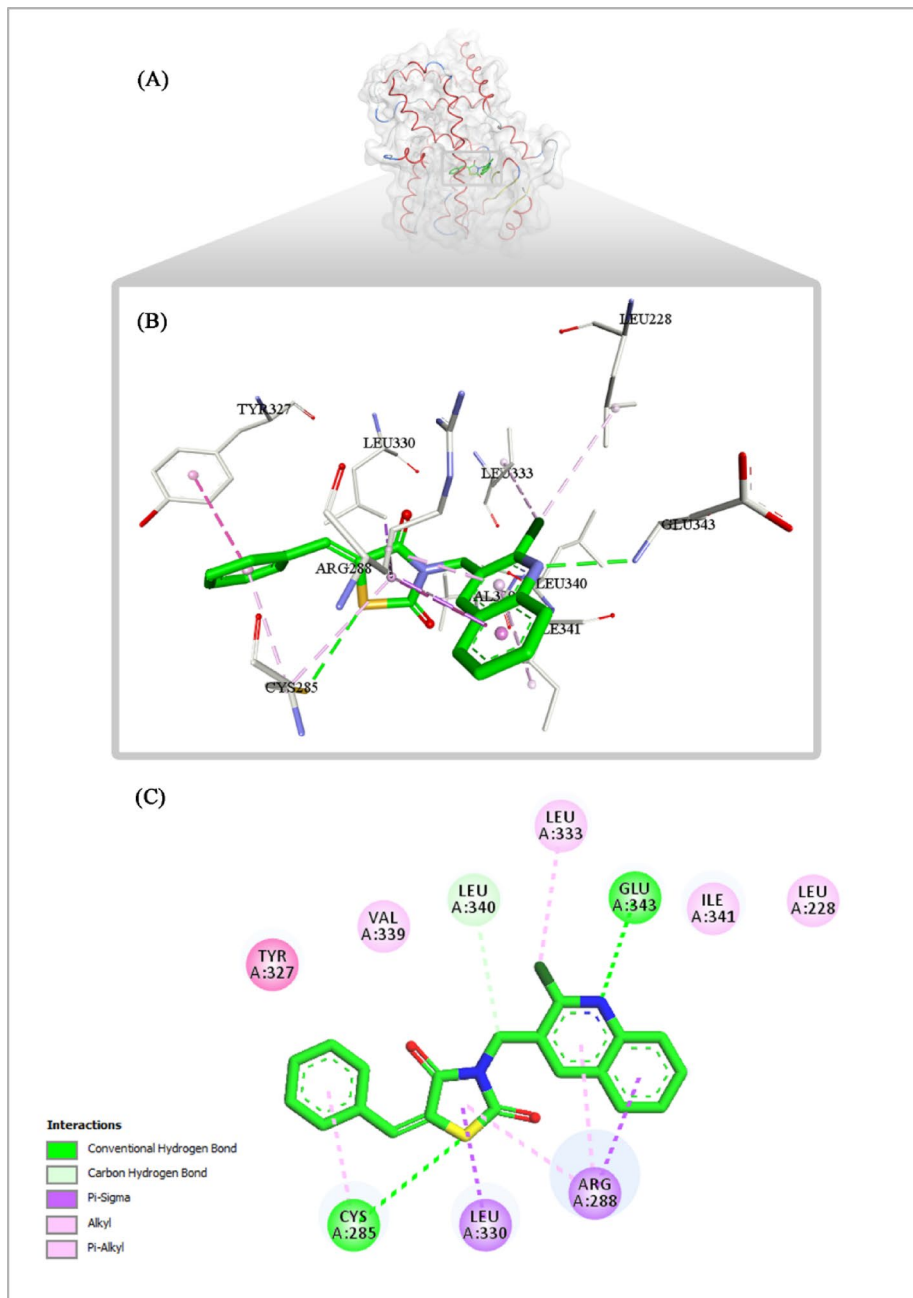


Fig. 17. (A) Overall structure of the PPAR γ LBD complexed with compound 7 (green); (B) 3D and (C) 2D binding mode of 7 with PPAR γ LBD.

aluminum sheets, using hexane/ethyl acetate (2:8) as the mobile phase. TLC spots were visualized under UV light (254/365 nm). Melting points of the synthesized compounds were determined by open glass capillary tubes and are uncorrected. The ^1H NMR and ^{13}C NMR spectra were recorded on Bruker model DRX-500 and 100 MHz, respectively, in $\text{DMSO}-d_6$ using tetramethylsilane (TMS) as the internal standard. Chemical shift values are given in δ (ppm) and the signals are described as s (singlet), d (doublet), t (triplet), q (quartet), and m (multiplet) whereas coupling constants (J) are expressed in Hz. Mass spectra were recorded on an Advion Compact Mass Spectrometer (CMS) using electrospray ionization (ESI) with amlodipine as standard. HPLC analysis was performed on an Agilent 1260 Infinity II system using 100% acetonitrile as the mobile phase.

Synthesis of 2-chloroquinoline-3-carbaldehyde 1

Yellow crystals, (4.1 gm) 42% yield, m.p.: 144–146 °C (lit. m.p.: 146–148 °C)³⁷.

Synthesis of (2-chloroquinolin-3-yl)methanol 2

White powder, (0.35 gm) 91% yield, m.p.: 166–167 °C (lit. m.p.: 166–168 °C)³⁸.

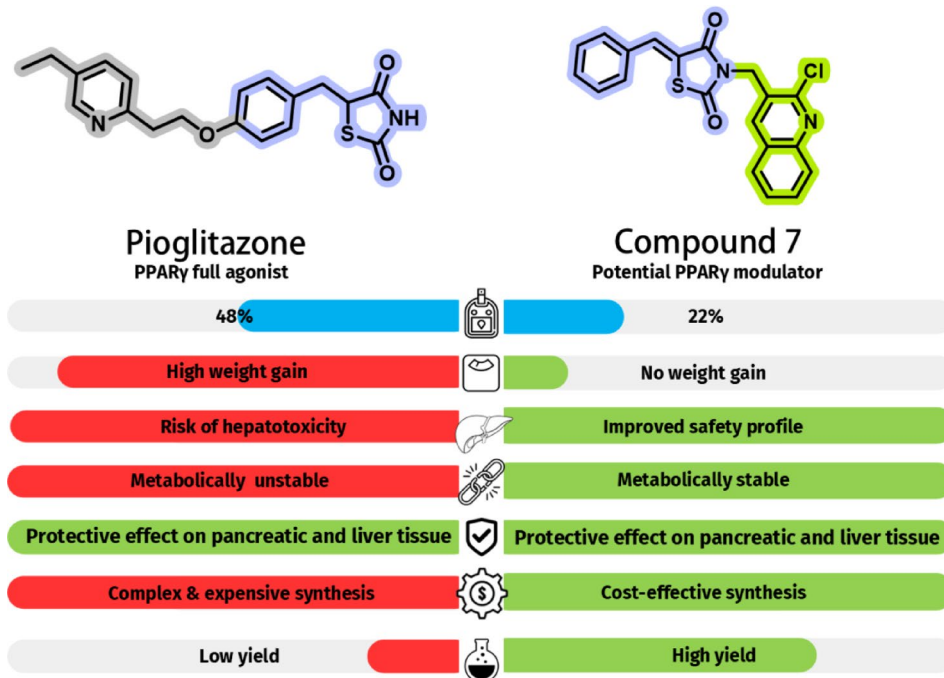


Fig. 18. Comparative summary of biological and synthetic profiles of PIO and compound 7.

Synthesis of 2-chloro-3-(chloromethyl)quinoline 3

Light brown crystals, (0.293 gm) 92% yield; m.p.: 115–116 °C (lit. m.p.: 116–117 °C)³⁸.

Synthesis of 1,3-thiazolidine-2,4-dione 4

White crystals, (5.69 gm) 81% yield, m.p.: 126–127 °C (lit. m.p.: 125–127 °C)³⁹.

Synthesis of (Z)-5-benzylidenethiazolidine-2,4-diones 5

Pale yellow powder, (0.32 gm) 78% yield, m.p.: 237–238 °C (lit. m.p.: 237–238 °C)⁴⁰.

Synthesis of (Z)-5-benzylidene-1,3-thiazolidine-2,4-dione potassium salt 6

White powder, (0.276 gm) 76% yield, m.p.: >300 °C.

Synthesis of (Z) 5-benzylidene-3-[(2-chloroquinolin-3-yl)methyl]thiazolidine-2,4-diones 7

Potassium salt of (Z)-5-benzylidenethiazolidine-2,4-dione **6** (1 mmol, 0.243 gm) was added to a stirred solution of intermediate **3** (1 mmol, 0.212 gm) in acetonitrile (50 mL) and heated under reflux. The progress of the reaction was monitored by TLC using 3:7 hexane : ethyl acetate as eluent. After the completion of the reaction, the solvent was evaporated under reduced pressure. Then, the residue was added to water, the formed precipitate was filtered off, washed with water, dried, and recrystallized from acetonitrile. White crystals, (0.239 gm) 63% yield, m.p.: 235–236 °C; ^1H NMR (500 MHz, DMSO- d_6) δ 8.40 (s, 1 H, quinoline H4), 8.03 (d, J =8.1 Hz, 1 H, quinoline H5), 7.97 (s, 1 H, methine C-H), 7.94 (d, J =8.4 Hz, 1 H, quinoline H8), 7.79 (m, 1 H, quinoline H7), 7.64 (m, 3 H, phenyl 2 H and quinoline H6), 7.54 (m, 2 H, phenyl), 7.49 (m, 1 H, phenyl), 5.00 (s, 2 H, CH_2); ^{13}C NMR (100 MHz, DMSO- d_6) δ 167.41, 165.50, 148.25, 146.28, 137.31, 133.38, 132.95, 130.96, 130.78, 130.19, 129.45, 127.99, 127.62, 127.51, 126.88, 126.50, 121.38, 42.60; HPLC analysis: Mobile phase: 100% MeCN, Retention Time (RT): 2.395 min, peak area: 94.89% at λ^{\max} 236 nm; ESI-MS m/z: 380.5 [M+H]⁺ (calcd. for $\text{C}_{21}\text{H}_{14}\text{ClN}_2\text{O}_2\text{S}$, 380.86).

Biological investigation

In vivo antidiabetic activity

In vivo antidiabetic study was determined by studying the effect of orally administered compound **7** on glucose tolerance on alloxan-induced non-insulin-dependent diabetes mellitus (NIDDM) in rats³³. Twenty adult healthy male Albino Wistar rats (170–200 gm) were acquired from Deraya University, Minia, Egypt, and kept at room temperature with food and water *ad libitum*. Alloxan was freshly prepared in normal saline solution for inducing diabetes at a dose of 120 mg/kg body weight intraperitoneally to fifteen overnight-fasted rats, after 3 days of acclimatization. To overcome drug-induced hypoglycemia, the animals were permitted to drink only 5% glucose solution the whole night. The remaining five rats were injected with an equivalent volume of CMC as the normal control group (Group I). BGL was measured after 72 h for all rats using glucometer. Rats were considered diabetic when their BGL was found to be at least 250 mg/dL.²⁶ Diabetic rats were then divided into three groups (five rats each). Diabetic control group (Group II) was only given the vehicle (0.25% CMC) orally. Diabetic rats

were orally fed with PIO (Diabetin tablets, Unipharma^{*}) as 0.25% CMC suspension at a dose of 36 mg/kg (Group III). Diabetic rats were orally fed with synthesized compound 7 (as 0.25% CMC suspension) at an equimolar dose (38 mg/kg) of the reference drug PIO (Group IV). BGLs were then measured at 0, 1, 7, and 15 days by collecting blood samples from the tail vein (caudal vein)⁴¹. The percentage of change in blood glucose level was calculated using the following formula⁴².

$$\% \text{ lowering of blood glucose level} = (C_F - C_L) / C_F \times 100.$$

C_F is the blood glucose concentration on day 0, and C_L is the blood glucose concentration after 15 days.

Overnight-fasted rats were weighed using an electric balance prior to the commencement of the study, and their weights were recorded on day 15 for body weight gain study.

After the end of the experiment, animals were euthanized using an overdose of Ketamine-Xylazine (300 mg/kg and 36 mg/kg, respectively) administered intraperitoneally. This method ensured that the animals were rendered unconscious and insensible to pain prior to sacrifice. Following confirmation of deep anesthesia through absence of pedal reflex and the induction of anesthesia, the animals were humanely sacrificed, and terminal blood collection was performed *via* cardiac puncture. Plasma samples were then collected for biochemical analysis. Pancreas was collected and divided into two portions. One portion for studying morphological changes in pancreatic tissue. The other portion of pancreas was freshly extracted with TRIzol™ reagent for total RNA. All animal experiments were approved by the Institutional Animal Ethics Committee (Approval No. 12/2023) at Deraya university. The study was conducted in accordance with the relevant guidelines and regulations, including National Institutes of Health (NIH) guidelines. Additionally, all procedures followed the ARRIVE (Animal Research: Reporting of In Vivo Experiments) guidelines to ensure proper reporting of in vivo studies.

PPAR γ gene expression study

An ultrasonic homogenizer (Sonics-Vibracell, Sonics & Materials Inc., Newtown, USA) was used to homogenize 100 mg of pancreatic tissue in 1 mL of TRIzol™ solution (Amresco, Solon, USA). Total RNA was isolated from pancreatic tissues using the TRIzol™ RNA extraction reagent (Amresco, Solon, USA) according to the manufacturer's instructions. The total RNA concentration was assessed at A₂₆₀ nm, and the purity was computed using the A₂₆₀/A₂₈₀ ratio. When purity of the samples ≥ 1.7 , samples were used for qRT-PCR utilizing GAPDH (Glyceraldehyde-3-phosphate dehydrogenase) as a reference housekeeping gene for determining the relative expression of PPAR γ .

The RevertAid H Minus First Strand cDNA Synthesis kit (#K1632, Thermo Scientific Fermentas, St. Leon-Ro, Germany) was used to synthesize cDNA for equivalent amounts of total RNA in all samples, according to the manufacturer's instructions. Single-stranded cDNAs were used in real-time PCR. SYBER Green [#K0251, Thermo Scientific Fermentas St. Leon-Ro, Germany-Maxima SYBER Green qPCR Master Mix (2X)] was used for PCR reactions and the StepOne Real-Time PCR Detection System (Applied Biosystems) was also used. Real-time polymerase chain reaction (qRT-PCR) was performed with 20 μ L of RealMOD Green qRT-PCR Mix kit (iNtRON biotechnology) containing 0.02 μ g RNA per reaction and 10 Pmol of specified primers for 30 cycles of 95 °C for 10 s. and 60 °C for 1 min. To assess the relative quantities of the products, the comparative threshold cycle (C_t) approach was utilized. The formula 2^(-ΔΔCt) was used to determine the relative expression. They were scaled in relation to controls, with control samples set to a value of one. The PPAR γ primers used for rat-specific PPAR γ were (forward: 5'- GCA TGG TGC CTT CGC TGA TG -3'; reverse: 5'- AGA ATA ATA AGG CGG CGG CGC -3') and GenBank accession number is NM_013124.3.

Hepatotoxicity studies

The collected samples of serum ALT and AST of the mice were quantified with ALT assay kits, according to the manufacturers' protocols⁴³.

Predicted metabolites of 7 were generated using the web-based GLORYx tool (<https://nerdd.univie.ac.at/gloryx/>), University of Hamburg, Germany, simulating phase I and phase II metabolic reactions in humans using machine learning and site-of-reaction-based prediction models³¹. This was achieved by using the "phase I and II metabolism" option following the generation of SMILE notation using ChemDraw. Results from phase I and II metabolites with a corresponding score equal to or greater than 25% were selected.

Morphological changes in pancreatic tissue

One portion of pancreas was collected and stored in 10% neutral-buffered formalin, dehydrated in a graded ethanol series, cleared in xylene, and embedded in paraffin wax. Five Sects. (3–5 μ m thickness) were stained with H&E and then examined under microscope at 400x and 1000x magnification⁴⁴.

Statistical analysis

The data was encoded and entered using the Graph Pad Prism version 9 statistical package (Graph Pad, La Jolla, CA, USA). Statistical variations between groups were evaluated using one-way analysis of variance (ANOVA) followed by Bonferroni *t*-test. Results of all biological studies were expressed as means \pm SD. P-values less than 0.05, was considered statistically significant, **p*<0.05.

Molecular docking study

Molecular docking was performed using AutoDock. The crystal structure of PPAR γ was obtained from RCSB Protein Data Bank (<http://www.rcsb.org/>). The crystal structure 5Y2O was selected for docking studies as it met the criteria of high-resolution data, well-defined binding sites, and their association with the specific ligand of interest in our research⁴⁵. The input files for molecular docking were prepared using Discovery Studio (DS) 2016 client and AutoDock tools 4.2.6 bundled with MGL tools (version 1.5.7). Prior to docking, the protein structure was subjected to necessary cleaning procedures, which involved removing small molecular ligands,

heteroatoms, non-standard residues, and water molecules. The 3D structures of ligands were retrieved from ChemDraw as a single file in 3D-spatial data file (SDF) format. The structures of ligands were energy-minimized using a universal force field and saved in PDB format. Then, these files were imported to Autodock, the Gasteiger charges and polar hydrogens were added, and the ligands were set up for the rotatable bond. The prepared protein and ligand files were then converted into PDBQT format, which serves as an input file for AutoDock for molecular docking. The binding site of the ligand was chosen according to a literature survey and selected as the active grid center. The dimensions of grid box were chosen to include all atoms of the ligands, default parameters were utilized with a grid box ($74 \times 60 \times 82$) Å which centered at (-47.217 \times -1.288 \times 77.334) Å with 0.375 Å of grid spacing. Additionally, the docking process was validated using co-crystallized ligand to ensure its quality and reliability for subsequent docking studies and the RMSD was calculated using LigRMSD server (<https://igrmrds.appsbio.utalca.cl/>). The molecular docking was proceeded using tested ligand and the protein-ligand conformation with the lowest binding energy was chosen and visualized by DS 2016 client.

In silico ADME prediction

The ADME properties of compound 7 were predicted using the SwissADME online tool (<http://swissadme.ch/>)³⁶. Molecular descriptors, pharmacokinetics, lipophilicity, and water solubility were analyzed to assess oral drug-likeness.

Conclusion

In this study, we successfully designed, synthesized, and evaluated compound 7, a novel quinoline-thiazolidinedione hybrid, as a potential SPPARM with improved safety and therapeutic potential for diabetes management. Compound 7 demonstrated effective antidiabetic activity, effectively lowering blood glucose levels while exhibiting a safer metabolic and histopathological profile compared to PIO. Notably, compound 7 showed lower hepatotoxicity, minimal weight gain, and enhanced metabolic stability, addressing key safety concerns associated with traditional thiazolidinediones. Furthermore, its protective effects on liver and pancreatic tissues highlight its potential as a safer therapeutic option.

Molecular docking studies confirmed the strong binding affinity of compound 7 to PPAR γ , interacting with key amino acid residues within the PPAR γ LBD. These findings support its role as a potential selective PPAR γ modulator, capable of dissociating insulin-sensitizing effects from adverse side effects. Additionally, ADME predictions indicated that compound 7 complies with Lipinski's rule of five, with no violations, suggesting favorable oral bioavailability and high gastrointestinal GI absorption, making it suitable for oral administration.

While our findings demonstrate the promising potential of compound 7, certain limitations should be acknowledged. Direct PPAR γ binding assays are essential for measuring its efficacy and comparing it with other partial agonists. Moreover, while computational ADME predictions provide valuable insights into compound 7's pharmacokinetic profile, further experimental pharmacokinetic studies are important to validate these findings and fully characterize ADME properties. These studies are planned as part of our future work to further explore its pharmacological potential.

Data availability

The datasets generated and analyzed during the current study are available from the corresponding author upon reasonable request. All relevant data supporting the findings of this study, including synthetic procedures, in vivo experimental results, NMR spectra, and HPLC chromatograms are included in the manuscript and its supplementary information files. Additional raw data such as molecular docking files, can be provided by the corresponding author upon request.

Received: 4 February 2025; Accepted: 20 May 2025

Published online: 01 June 2025

References

- DeFronzo, R. A. et al. Type 2 diabetes mellitus. *Nat. Rev. Dis. Primers.* **1**, 15019 (2015).
- Yki-Järvinen, H. Thiazolidinediones. *N. Engl. J. Med.* **351**, 1106–1118 (2004).
- Yau, H., Rivera, K., Lomonaco, R. & Cusi, K. The future of thiazolidinedione therapy in the management of type 2 diabetes mellitus. *Curr. Diab. Rep.* **13**, 329–341 (2013).
- Kahn, S. E. et al. Glycemic durability of rosiglitazone, metformin, or glyburide monotherapy. *N. Engl. J. Med.* **355**, 2427–2443 (2006).
- Soccio, R. E., Chen, E. R. & Lazar, M. A. Thiazolidinediones and the promise of insulin sensitization in type 2 diabetes. *Cell. Metab.* **20**, 573–591 (2014).
- Bansal, G., Thanikachalam, P. V., Maurya, R. K., Chawla, P. & Ramamurthy, S. An overview on medicinal perspective of thiazolidine-2,4-dione: A remarkable scaffold in the treatment of type 2 diabetes. *J. Adv. Res.* **23**, 163–205 (2020).
- Ahmadian, M. et al. PPAR γ signaling and metabolism: the good, the bad and the future. *Nat. Med.* **19**, 557–566 (2013).
- Rosen, E. D. & Spiegelman, B. M. PPAR γ : A nuclear regulator of metabolism, differentiation, and cell growth. *J. Biol. Chem.* **276**, 37731–37734 (2001).
- Mangelsdorf, D. J. & Evans, R. M. The RXR heterodimers and orphan receptors. *Cell* **83**, 841–850 (1995).
- Schoonjans, K., Staels, B. & Auwerx, J. The peroxisome proliferator activated receptors (PPARS) and their effects on lipid metabolism and adipocyte differentiation. *Biochim. Biophys. Acta* **1302**, 93–109 (1996).
- Saltiel, A. R. & Olefsky, J. M. Thiazolidinediones in the treatment of insulin resistance and type II diabetes. *Diabetes* **45**, 1661–1669 (1996).
- Nolte, R. T. et al. Ligand binding and co-activator assembly of the peroxisome proliferator-activated receptor-gamma. *Nature* **395**, 137–143 (1998).
- Lincoff, A. M., Wolski, K., Nicholls, S. J. & Nissen, S. E. Pioglitazone and risk of cardiovascular events in patients with type 2 diabetes mellitus: a meta-analysis of randomized trials. *JAMA* **298**, 1180–1188 (2007).
- Tang, H. et al. Pioglitazone and bladder cancer risk: a systematic review and meta-analysis. *Cancer Med.* **7**, 1070–1080 (2018).

15. Tuccori, M. et al. Pioglitazone use and risk of bladder cancer: population based cohort study. *BMJ.* **352** (2016).
16. Gelman, L., Feige, J. N. & Desvergne, B. Molecular basis of selective PPAR γ modulation for the treatment of type 2 diabetes. *Biochim. Et Biophys. Acta (BBA) - Mol. Cell. Biology Lipids.* **1771**, 1094–1107 (2007).
17. Higgins, L. S. & Depaoli, A. M. Selective peroxisome proliferator-activated receptor γ (PPAR γ) modulation as a strategy for safer therapeutic PPAR γ activation. *Am. J. Clin. Nutr.* **91**, 267S–270S (2010).
18. Motani, A. et al. INT131: a selective modulator of PPAR gamma. *J. Mol. Biol.* **386**, 1301–1311 (2009).
19. Taxak, N., Parmar, V., Patel, D. S., Kotasthane, A. & Bharatam, P. V. S-oxidation of thiazolidinedione with hydrogen peroxide, peroxy nitrous acid, and c4a-hydroperoxyflavin: A theoretical study. *J. Phys. Chem. A.* **115**, 891–898 (2011).
20. Campos, M. L. et al. New pioglitazone metabolites and absence of opened-ring metabolites in new N-substituted thiazolidinedione. *Drug Metab. Dispos.* **46**, 879–887 (2018).
21. Mohamed, M. F. A. & Abuo-Rahma, G. E. D. A. Molecular targets and anticancer activity of quinoline-chalcone hybrids: literature review. *RSC Adv.* **10**, 31139–31155 (2020).
22. Ibrahim, A. M. et al. Chemistry and applications of functionalized 2,4-thiazolidinediones. *Eur. J. Org. Chem.* **26**, e202300184 (2023).
23. Sohda, T. et al. Studies on antidiabetic agents. II. Synthesis of 5-[4-(1-methylcyclohexylmethoxy)-benzyl]thiazolidine-2,4-dione (ADD-3878) and its derivatives. *Chem. Pharm. Bull. (Tokyo).* **30**, 3580–3600 (1982).
24. Madivada, L. R. et al. An improved process for pioglitazone and its pharmaceutically acceptable salt. *Org. Process. Res. Dev.* **13**, 1190–1194 (2009).
25. Nazreen, S. et al. Design, synthesis, in silico molecular docking and biological evaluation of novel oxadiazole based thiazolidine-2,4-diones bis-heterocycles as PPAR- γ agonists. *Eur. J. Med. Chem.* **87**, 175–185 (2014).
26. Naim, M. J. et al. Synthesis, docking, in vitro and in vivo antidiabetic activity of pyrazole-based 2,4-thiazolidinedione derivatives as PPAR- γ modulators. *Arch. Pharm. (Weinheim).* **351**, e1700223 (2018).
27. Kroker, A. J. & Bruning, J. B. Review of the structural and dynamic mechanisms of PPAR γ partial agonism. *PPAR Res.* **2015** (2015).
28. Reddy, V. B. G. et al. Mechanistic studies on the metabolic scission of thiazolidinedione derivatives to acyclic thiols. *Chem. Res. Toxicol.* **18**, 880–888 (2005).
29. Shen, Z. et al. Identification of novel metabolites of pioglitazone in rat and dog. *Xenobiotica* **33**, 499–509 (2008).
30. Alvarez-Sánchez, R., Montavon, F., Hartung, T. & Pähler, A. Thiazolidinedione bioactivation: A comparison of the bioactivation potentials of troglitazone, rosiglitazone, and Pioglitazone using stable isotope-labeled analogues and liquid chromatography tandem mass spectrometry. *Chem. Res. Toxicol.* **19**, 1106–1116 (2006).
31. De Bruyn Kops, C., Šicho, M., Mazzolari, A. & Kirchmair, J. GLORYX: Prediction of the metabolites resulting from phase 1 and phase 2 biotransformations of xenobiotics. *Chem. Res. Toxicol.* **34**, 286–299 (2021).
32. Ramadan, B. K., Schaalan, M. F. & Tolba, A. M. Hypoglycemic and pancreatic protective effects of Portulaca oleracea extract in alloxan induced diabetic rats. *BMC Complement. Altern. Med.* **17**, (2017).
33. Igohodaro, O. M., Adeosun, A. M. & Akinloye, O. A. Alloxan-induced diabetes, a common model for evaluating the glycemic-control potential of therapeutic compounds and plants extracts in experimental studies. *Med. (B Aires).* **53**, 365–374 (2017).
34. Kimura, T. et al. Protective effects of pioglitazone and/or liraglutide on pancreatic β -cells in Db/db mice: comparison of their effects between in an early and advanced stage of diabetes. *Mol. Cell. Endocrinol.* **400**, 78–89 (2015).
35. Gampe, R. T. et al. Asymmetry in the PPARgamma/RXRalpha crystal structure reveals the molecular basis of heterodimerization among nuclear receptors. *Mol. Cell.* **5**, 545–555 (2000).
36. Daina, A., Michielin, O. & Zoete, V. SwissADME: a free web tool to evaluate pharmacokinetics, drug-likeness and medicinal chemistry friendliness of small molecules. *Sci. Rep.* **7**(1), 1–13 (2017).
37. Salahuddin, Mazumder, A. & Shaharyar, M. Synthesis, antibacterial and anticancer evaluation of 5-substituted (1,3,4-oxadiazol-2-yl)quinoline. *Med. Chem. Res.* **24**, 2514–2528 (2015).
38. Bokosi, F. R. B. et al. Design, synthesis and biological evaluation of mono- and bisquinoline methanamine derivatives as potential antiplasmoidal agents. *Bioorg. Med. Chem. Lett.* **38**, 127855 (2021).
39. Elkholi, N. et al. Discovery of 3-(2-aminoethyl)-thiazolidine-2,4-diones as a novel chemotype of sigma-1 receptor ligands. *Chem. Biol. Drug Des.* **100**, 25–40 (2022).
40. Meirelles, L. V. et al. Diverse 3-methylthio-4-substituted maleimides through a novel rearrangement reaction: synthesis and selective cell imaging. *J. Org. Chem.* **87**, 2809–2820 (2022).
41. Togashi, Y. et al. Evaluation of the appropriateness of using glucometers for measuring the blood glucose levels in mice. *Sci. Rep.* **6**, 25465 (2016).
42. Candasamy, M., Murthy, T. E. G. K., Gubiyappa, K. S., Chellappan, D. K. & Gupta, G. Alteration of glucose lowering effect of glibenclamide on single and multiple treatments with fenofibrate in experimental rats and rabbit models. *J. Basic. Clin. Pharm.* **5**, 62 (2014).
43. Naim, M. J. et al. Synthesis, molecular docking and anti-diabetic evaluation of 2,4-thiazolidinedione based amide derivatives. *Bioorg. Chem.* **73**, 24–36 (2017).
44. Lambert, J. D. et al. Hepatotoxicity of high oral dose (-)-epigallocatechin-3-gallate in mice. *Food Chem. Toxicol.* **48**, 409 (2010).
45. Lee, M. A., Tan, L., Yang, H., Im, Y. G. & Im, Y. J. Structures of PPAR complexed with lobeglitazone and pioglitazone reveal key determinants for the recognition of antidiabetic drugs. *Sci. Rep.* **7**, 16837 (2017).

Acknowledgements

I would like to thank my colleague: Sara Nabil Shokrany, Medical Biochemistry Department, Faculty of Post-graduates Studies for Advanced Science, Beni-Suef University, for providing me with the PPAR γ qRT-PCR primers for the completion of PPAR γ gene expression study.

Author contributions

Ayman M. Ibrahim: Methodology, Investigation, Formal Analysis, Writing – Original Draft, Visualization. Mai E. Shoman: Writing – Review & Editing. Radwa Taher Mohie el-dien: Investigation, Formal Analysis (HPLC). Entesar Ali Saber: Investigation, Formal Analysis (Histopathology). Mahmoud Abdelnaser: Investigation, Formal Analysis (PPAR γ gene expression and liver enzymes). Sherif A. Maher: Formal Analysis (Statistical Analysis), Validation. Alaa M. Hayallah: Conceptualization, Supervision, Project Administration, Writing – Review & Editing. Mahmoud Abdul-Aziz El-Rehany: Conceptualization, Supervision, Review & Editing (Biological evaluation). Gamal El-Din A. Abuo-Rahma: Conceptualization, Supervision, Project Administration, Writing – Review & Editing.

Funding

Open access funding provided by The Science, Technology & Innovation Funding Authority (STDF) in cooperation with The Egyptian Knowledge Bank (EKB).

Declarations

Competing interests

The authors declare no competing interests.

Additional information

Supplementary Information The online version contains supplementary material available at <https://doi.org/10.1038/s41598-025-03387-9>.

Correspondence and requests for materials should be addressed to A.M.H. or G.E.-D.A.A.-R.

Reprints and permissions information is available at www.nature.com/reprints.

Publisher's note Springer Nature remains neutral with regard to jurisdictional claims in published maps and institutional affiliations.

Open Access This article is licensed under a Creative Commons Attribution 4.0 International License, which permits use, sharing, adaptation, distribution and reproduction in any medium or format, as long as you give appropriate credit to the original author(s) and the source, provide a link to the Creative Commons licence, and indicate if changes were made. The images or other third party material in this article are included in the article's Creative Commons licence, unless indicated otherwise in a credit line to the material. If material is not included in the article's Creative Commons licence and your intended use is not permitted by statutory regulation or exceeds the permitted use, you will need to obtain permission directly from the copyright holder. To view a copy of this licence, visit <http://creativecommons.org/licenses/by/4.0/>.

© The Author(s) 2025